



Analysis of a High Accuracy Service based on JPL's Global Differential GPS

Nacer Naciri¹ | Yoaz Bar-Sever¹ | Willy Bertiger¹ | Sunil Bisnath² | Attila Komjathy¹ | Mark Miller¹ | Larry Romans¹ | Bela Szilagyi¹ | Michele Vallisneri¹

¹ Jet Propulsion Laboratory, California Institute of Technology, Pasadena, California, USA

² Department of Earth and Space Science and Engineering, York University, Toronto, ON, Canada

Correspondence

Nacer Naciri
4800 Oak Grove Dr, Pasadena,
CA 91109, USA.
Email: nacer.naciri@jpl.nasa.gov

Abstract

In the current global navigation satellite system (GNSS) context, with several constellations offering high accuracy services (HAS), we have evaluated a potential HAS for GPS based on JPL's Global Differential GPS (GDGPS) system. This HAS also provides corrections for Galileo and GLONASS. In this paper, we specifically consider the scenario in which satellite corrections are delivered to users through the internet, similar to one style of access used for Galileo HAS. The GDGPS-based HAS described herein consists primarily of high-quality satellite orbit and clock corrections and currently excludes code and phase biases. Corrections are provided in two parallel variations: one stream supporting GPS and Galileo, and the other supporting GPS and GLONASS. Each variation is provided in two redundant instances for robustness, giving a total of four streams. Our results, including PPP solutions based on these products, attest to the quality of the corrections. PPP results show good performance, comparable to solutions generated based on real-time CNES products and better than solutions generated based on internet-based Galileo HAS products. For example, based on processing over 2,000 independent three-hour data sets, both the GDGPS-based HAS GPS+GAL streams and the CNES stream achieved post-convergence horizontal rms below 20 cm for 97% of data sets and below 10 cm for 80%. In contrast, only 86% of Galileo HAS-based solutions have post-convergence horizontal rms below 20 cm, and only 47% have rms below 10 cm. Overall, these results suggest a promising method of implementing a GDGPS-based HAS that might augment GPS, Galileo, and GLONASS.

Keywords

Galileo, GDGPS, GLONASS, GPS, high accuracy service, PPP

1 | INTRODUCTION

Global navigation satellite systems (GNSSs) began with the launch of the Global Positioning System (GPS) constellation, which became fully operational in 1993 (NASA, 2023). The GPS system was initially designed for military applications; when it was first released for civilian use, its signals were intentionally degraded, limiting the accuracy to hundreds of meters for real-time users who lacked the

benefit of differential corrections. In May 2000, this intentional degradation, known as selective availability, was turned off, instantaneously reducing position errors to the meter level for civil users (GPS.gov, 2021). Another GNSS, the Russian constellation GLONASS, was also designed for military use and declared operational in the same year as GPS, though it did not become fully operational until 1995 (GLONASS IAC, n.d.). GLONASS's use of a frequency division multiple access (FDMA) frequency structure instead of a code division multiple access (CDMA) as in GPS limited the use of the former by civil users. The constellation degraded to the point where only seven satellites were operational in 2002, falling behind GPS.

As the importance of GPS became obvious to an increasing number of civilian and military applications, other GNSS constellations started emerging and GLONASS was modernized. Today, the two other global constellations are the European Union's Galileo, which entered into service in December 2016 (Falcone et al., 2017), and China's BeiDou, which consists of two different versions. BeiDou-2 has provided positioning services in the Asia-Pacific region since December 2012, while BeiDou-3 has provided global service since 2023 (Yang et al., 2019). While all four constellations enable positioning for users anywhere on Earth, other regional constellations that offer more local positioning and augmentation have also been launched, including Japan's quasi-zenith satellite system (QZSS) and the Indian regional navigation satellite system (IRNSS or NavIC).

The GNSS constellations were designed with meter-level positioning in mind: receivers track signals from each satellite and compute the travel time of each signal. Then, thanks to broadcast satellite orbit and clock states in the navigation message, users can geometrically interpret the signals and use a form of trilateration to estimate their position within a few meters. More precise (i.e., decimeter to centimeter-level) positioning has only appeared and evolved after the fact with the emergence of techniques such as real-time kinematic (RTK) and precise point positioning (PPP). These techniques rely on reference stations with known precise positions, with the reference station data being used to further eliminate errors and augment the broadcast-based solution. For example, RTK is based on the presence of a reference station in the vicinity of the user. Data from the reference station is transmitted to the user in the observation space, allowing for centimeter-level positioning after double-differencing between the receivers and satellites. A variant called network RTK (NRTK) is based on a network of nearby reference stations. NRTK initially started in an observation space representation (OSR), similar to RTK, but it has since evolved to a state space representation (SSR) to reduce the bandwidth required for transmission correction. PPP also relies on a network of reference stations, similar to NRTK, but it uses a limited number of global stations. The global network is used to estimate precise satellite orbits, clocks, and biases, which are transmitted to the user and then used in a point positioning solution to achieve decimeter- to centimeter-level positioning. Overall, as more research and development have been performed on these two precise techniques, an increasing number of applications and correction providers have switched from OSR to SSR corrections regardless of whether the networks are global or regional. This shift is driven by the state representation's ease of use, low bandwidth requirements, and high performance. Because SSR corrections can be converted to the observation space, many providers also offer SSR to OSR converters to ensure compatibility with OSR-based hardware and software.

SSR corrections have traditionally been transmitted over the internet (IGS, 2023), geostationary satellites (Lundberg, 1995), or 4G/5G (Swift Navigation, 2020). Such means of transmission mean that users require a separate

communication protocol to receive SSR corrections in addition to the protocol for GNSS signals. Given the ever-increasing interest in and demand for precise positioning, the modernized versions of many positioning constellations include a precise positioning component in their navigation service. For example, Japan's QZSS has included its centimeter-level augmentation service since 2016, which provides QZSS, GPS, and Galileo PPP-RTK corrections over areas surrounding Japan (Miya et al., 2016). QZSS is also developing a modernized PPP service named multi-GNSS advanced orbit and clock augmentation (MADOCA) (Kawate et al., 2023). A similar regional PPP service, named PPP-B2b, has recently been established by BeiDou as part of its third generation BeiDou-3. This service broadcasts BeiDou and GPS SSR corrections to users in the Asia-Pacific region (Liu et al., 2020). While both QZSS's and BeiDou's PPP services are regional, Galileo recently became the first constellation with a global PPP service. Galileo's service, named high-accuracy service (HAS), provides precise SSR corrections to users around the world through a dedicated E6B signal (EUSPA, 2023). All three of these existing PPP services use a dedicated signal to transmit SSR corrections, with Galileo HAS including an additional internet-based distribution to complement the satellite-based distribution.

GPS remains the pioneering GNSS constellation in operation, but it lacks a high-accuracy service component and, unlike other constellations, does not currently have plans for a dedicated precise positioning signal. NASA's Jet Propulsion Laboratory (JPL) team has accumulated decades of experience working on the Global Differential GPS (GDGPS) system: a complete, accurate, and robust real-time GNSS monitoring and augmentation system. This system leverages NASA's real-time global GNSS network receivers and the cutting-edge geodetic software GipsyX/RTGx, which is capable of real-time precise orbit determination for GPS, GLONASS, BeiDou, Galileo, QZSS, and NAVIC (Bertiger et al., 2020; GDGPS, 2020). It also incorporates a suite of ancillary products, including integrity information and atmospheric data. The GDGPS system and its associated software already support critical applications such as the wide area augmentation system (WAAS) and the planned next-generation GPS operational control segment (OCX), alongside various commercial licenses.

This manuscript discusses a version of a GDGPS-based HAS service that could be used to augment GPS, Galileo, and GLONASS. It provides a detailed description of the corrections, their performance compared to reference post-processed sources, and the performance of independent PPP users with the current data streams. The proposed high-accuracy service is referred to as "GDGPS HAS" herein.

The manuscript starts with a description of the correction streams and the correction generation process, followed by an analysis of the precise corrections. This analysis includes internal comparisons, a comparison against reference external post-processed products, and a latency analysis. The manuscript then continues with a description of the PPP user processing strategies and data used, followed by a presentation of independent PPP results using the GDGPS HAS correction streams. The results are compared against other correction sources, namely Galileo HAS and the Centre National d'Etudes Spatiales (CNES). Finally, the manuscript ends with conclusions and future work.

2 | CORRECTION GENERATION PROCESS

The high precision products proposed herein as augmentation for GPS, GLONASS, and Galileo are based on the GDGPS system, which consists of multiple

hardware and software components. One key component of GDGPS is a global network of ground receivers used to collect observation and navigation data, which is transmitted to JPL-operated data centers for real-time processing. This network of ground receivers consists of:

- NASA-owned, JPL-operated GNSS receivers, which are called the global GNSS network (GGN) and funded by the space geodesy program (SGP). These are installed at approximately 60 sites.
- NASA-owned, JPL-operated GNSS receivers not funded by SGP, consisting of approximately 20 sites.
- Hundreds of additional publicly available sites provided by either the U.S. or international agencies such as the International GNSS Service (IGS).

Data from the JPL-operated receivers is either edited *in situ* using JPL software to avoid any issues affecting the editing, or it is edited after transmission and before processing. The data from each site is streamed to two JPL data centers currently being relocated to Pasadena, California and Las Vegas, Nevada. Both data centers comply with the Federal Information Security Modernization Act (FISMA) to conform to NASA's data cybersecurity requirements. The two geographically-separated data centers are fully independent and redundant, with independent processing, distribution, and internet service providers.

The GDGPS system is independent of local infrastructure, or user receiver and software. It has been used in a range of terrestrial, airborne, and spaceborne operations, such as precise orbit determination of low earth orbiters, and to support WAAS and OCX. The GDGPS system also supports timing applications in collaboration with national timing laboratories that provide real-time access to data from their monitoring sites.

The GDGPS system has provided high-accuracy, state-based corrections to commercial and government partners for many years (Bertiger et al., 1997; Whitehead et al., 1998). In order to provide highly accurate and precise satellite corrections, the GDGPS system relies on the GipsyX/RTGx software, which was developed at JPL and has been used for a multitude of geodetic applications (Bertiger et al., 2020). GipsyX/RTGx uses precise satellite force models and Earth models along with a square-root implementation of a Kalman filter to generate satellite orbits, clocks, and biases from observation data collected by the global network of receivers. To speed up the real-time estimation process, the estimation is separated into two filters running in parallel, as pictured in Figure 1:

- A slow filter estimates all the parameters at the one-minute rate. Parameters include satellite orbits, satellite clocks, ground clocks, and the troposphere. The slow filter uses ionosphere-free pseudorange and carrier-phase data from the network of ground stations.
- A fast filter runs at a one-second rate. Because the only parameters that change at this rate are clocks (space clocks are stable but may glitch, and many ground clocks are poor crystal oscillators), all parameters except clocks are propagated from the slow filter to the fast filter and held fixed. This structure allows data to be processed rapidly, with processing time adding less than one second to the nominal latency of data arrival. (This overall data latency is taken as 3 or 4 seconds in our system, which is quite generous in practice). The fast filter is based on carrier-phase measurements and does not use pseudorange measurements.

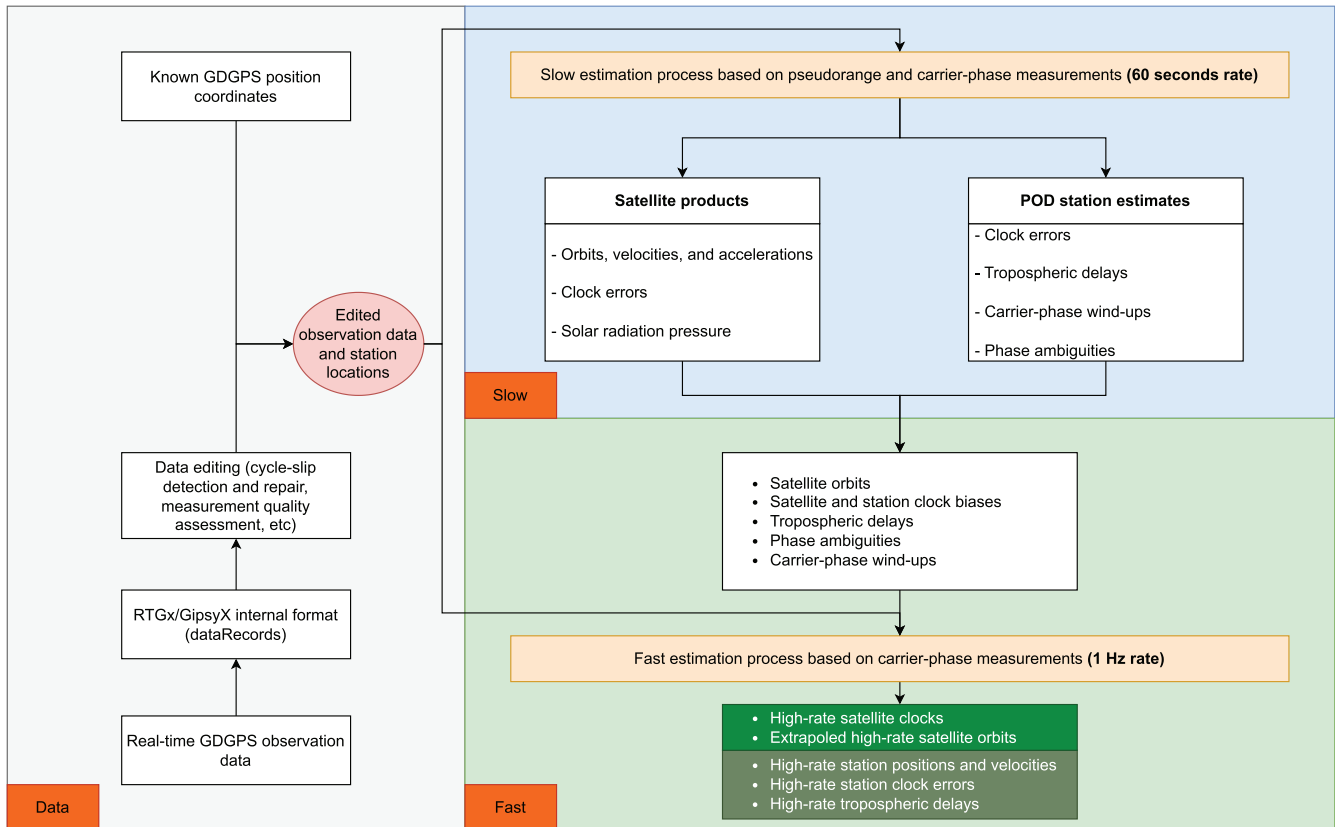


FIGURE 1 Diagram of the slow/fast process used to estimate precise satellite orbit and clock corrections.

In the case of GDGPS HAS, the satellite orbits and clocks estimated from the slow/fast processes are combined with the broadcast orbits and clocks to generate SSR corrections that can be transmitted to the user. Future versions of the streams will include full support for code and phase biases. The corrections are transmitted at a rate of 1 Hz in both Radio Technical Commission for Maritime Services (RTCM)-SSR and IGS-SSR formats, which are widespread open-source formats used to disseminate real-time corrections.

The GDGPS HAS service consists of three redundant streams, amounting to six streams in total, and each correction stream is based on an independent slow/fast filter pair as described above:

- Two GPS+Galileo streams, named **SSRA11JPL0** and **SSRA12JPL0**, provide 1 Hz precise orbit and clock corrections for GPS and Galileo satellites. The primary signals are L1 and L2 for GPS and E1 and E5b for Galileo. The two streams are generated by completely independent precise orbit determination (POD) filters located in geographically separate data centers.
- Two GPS+GLONASS streams, named **SSRA21JPL0** and **SSRA22JPL0**, provide 1 Hz precise orbit and clock corrections for GPS and GLONASS satellites. The primary signals are L1 and L2 for GPS and G1 and G2 for GLONASS. The two streams are generated by completely independent filters located in different data centers.
- Two broadcast ephemeris streams, named **BCEP01JPL0** and **BCEP02JPL0**, provide navigation messages for GPS, Galileo, and GLONASS to support the SSR correction streams described above.

Each pair of redundant streams is generated using independent filters that run on different data centers, but they are based on the same observation data coming from the GDGPS network and circulated between both data centers. This highly redundant architecture was developed by GDGPS over years to support users who need reliable, continuous GNSS services without single points of failure. It should be noted that, although the streams are redundant, they are not expected to be completely identical. Some discrepancies may arise due to the use of different machines with different processors, architectures, and configurations, which mainly dictates the configuration of the POD filters in terms of the numbers of reference stations and observable types to use, among other things. However, constant efforts are made to minimize the differences and have truly identical correction streams.

The GDGPS corrections analyzed herein are distributed via Crustal Dynamics Data Information System (CDDIS) and the IGS for scientific uses and are compatible with distribution to users over the internet, similar to what is available from Galileo HAS. As defined in (Bar-Sever et al., 2022), the GDGPS system achieves an orbital error rms below 15 cm for GPS and Galileo and 20 cm for GLONASS, along with clock error rms below 10 cm for GPS and Galileo and 15 cm for GLONASS. The user range error (URE) rms are typically expected to be below 8 cm for GPS and Galileo and below 12 cm for GLONASS. These accuracies are expected to translate to the GDGPS HAS streams, so similar product quality is anticipated.

3 | PRODUCTS ANALYSIS

In this section, orbits and clocks from each of the GPS+GLO and GPS+GAL (note: GLO=GLONASS, and GAL=Galileo) streams are analyzed via (i) comparisons against independent external products and (ii) an internal consistency check against highly precise JPL rapid products. The section concludes with analysis of the correction latency.

3.1 | Comparison against CODE final products

One way to analyze the quality of the orbit and clock corrections and to ensure consistency with other similar products is to compare orbits and clocks to those provided by independent IGS analysis centers. In this case, the GPS+GLO and GPS+GAL products are compared against final products from the Center for Orbit Determination in Europe (CODE) (Dach et al., 2020).

The CODE products are file-based, with orbits referring to the satellites' centers of mass and clocks referring to the ionosphere-free combination of L1/L2 for GPS, E1/E5a for Galileo, and G1/G2 for GLONASS. In contrast, GDGPS HAS orbits refer to the ionosphere-free antenna phase center at the primary frequencies, and GDGPS HAS clocks refer to the ionosphere-free combination of the primary frequencies. The primary frequencies for GDGPS HAS are L1/L2 for GPS, E1/E5b for Galileo, and G1/G2 for GLONASS. However, to compare the GDGPS HAS corrections to CODE, these differences in definitions must be accounted for. The CODE orbits are therefore moved to the respective antenna phase centers using the Antenna Exchange Format (ANTEX) IGS20 file (Villiger, 2022). The clock corrections are similarly aligned by applying differential code biases from the Chinese Academy of Sciences (CAS), which provides all the biases necessary for the alignment (Wang et al., 2016).

After the orbits are aligned, they can be transformed from an Earth-centered Earth-fixed (ECEF) frame to a satellite radial, along-track, and cross-track (RAC)

frame. In this frame, the along-track component is the unit vector ϵ_A following the satellite velocity; the cross-track component is the unit vector ϵ_C formed from the cross product of the satellite position and velocity; and the radial component is the unit vector ϵ_R that completes the orthogonal frame. The RAC (δA , δC , and δR , respectively) frame can be computed based on the GDGPS HAS and CODE ECEF differences using Equation (1):

$$\begin{bmatrix} \delta R \\ \delta A \\ \delta C \end{bmatrix} = \begin{bmatrix} \epsilon_R & \epsilon_A & \epsilon_C \end{bmatrix}^T \begin{bmatrix} X_{GDGPS} - X_{CODE} \\ Y_{GDGPS} - Y_{CODE} \\ Z_{GDGPS} - Z_{CODE} \end{bmatrix} \quad (1)$$

After the clock corrections are aligned, the clock comparison is simply the difference between the two sets of clocks: $\delta CLK = CLK_{GDGPS} - CLK_{CODE}$. However, clock references can be different between network providers, leading to shifts in the overall clock level for all satellites within each constellation. To counteract this effect, a mean clock per constellation is computed for each epoch and then removed from each satellite's individual clock. This approach results in an overall clock shift that reduces any common bias between each constellation's satellites. Such common biases do not affect user positioning because they get absorbed by receiver clocks. In addition, GLONASS is known for the presence of inter-signal biases (Håkansson et al., 2017), which appear as biases between individual satellites. To remove such inter-signal biases, the mean of the clock for each satellite on each day is subtracted from each satellite's clocks.

An additional metric used to compare products is the URE, which relates the quality of products to their potential impact on user positioning. While a site-specific URE metric already exists, the global average URE can be derived (Chen et al., 2002). The URE computation is detailed in Equation (2):

$$URE = \sqrt{(\delta R - \delta CLK)^2 + 0.0192(\delta A^2 + \delta C^2)} \quad (2)$$

Table 1 summarizes the rms of the differences between GDGPS HAS and CODE in the radial, along-track, and cross-track components, as well as clocks and URES. Each element in the table is generated based on seven days of data collected in late September and early October 2024 at five-minute intervals. Table 1 shows good performance from all products, with rms values below the decimeter level. However, a select few satellites (R730, R806, and R861 for SSRA21JPL0 (GPS+GLO) and R730

TABLE 1

Comparison of GDGPS HAS streams to final products from CODE. Values represent the rms in centimeters over seven days. URE values in parentheses refer to rms computed after removal of three misconfigured outlier satellites (R730, R806, and R861).

	SSRA11JPL0		SSRA12JPL0		SSRA21JPL0		SSRA22JPL0	
	GPS	GAL	GPS	GAL	GPS	GLO	GPS	GLO
Radial	2.7	7.9	2.9	7.6	2.7	8.7 (5.3)	3.0	8.6 (5.6)
Along-track	3.7	6.3	4.0	5.3	4.2	12.0 (7.0)	5.3	11.1 (7.9)
Cross-track	2.6	4.5	2.9	3.8	7.6	6.1 (4.6)	3.5	6.4 (5.4)
Clock	7.2	8.5	7.2	8.2	7.6	9.9 (6.8)*	7.6	6.4 (6.7)*
URE	6.1	6.9	6.0	6.9	6.4	10.1 (4.7)*	6.0	6.9 (4.9)*

* Note: The mean clock per satellite per day is removed from GLONASS clocks to avoid the effect of inter-signal biases. By contrast, a mean clock per constellation per epoch is removed for GPS and Galileo.

for SSRA22JPL0 (GPS+GLO)) had either higher radial or clock differences, leading to higher overall rms in the table. These outlier values are discussed in more detail in relation to Figure 2 below, and the rms values after these outliers were removed are shown in parentheses in Table 1.

Comparing rms values among different streams shows consistent performance across the streams. In the case of GPS, radial differences are ~ 2.7 cm across all four correction streams, and clock differences are ~ 7.5 cm. Likewise, the GPS UREs range between 6 cm and 6.4 cm across all four corrections streams. Such URE values are equivalent to GPS UREs for BeiDou's PPP-B2b service, as shown in Tang et al., 2022, though this previous study did not account for satellite clock differences in their URE computation and only focused on orbital corrections. The GPS URE values for GDGPS HAS reported here are also better than the signal-in-space range error (SISRE) values for Galileo HAS shown in Naciri et al., 2023. Note that these comparisons against BeiDou PPP-B2b and Galileo HAS are provided only to contextualize GDGPS HAS UREs among other similar, published values; rigorous URE comparison on the same data has not been performed.

In the case of Galileo, the quality of the corrections is also comparable between the two GPS+GAL streams (SSRA11JPL0 and SSRA12JPL0), with radial and clock differences of approximately 8 cm. The along-track and cross-track differences are higher for the SSRA12JPL0 stream compared to SSRA11JPL0, though these individual orbit and clock components nevertheless translate to a similar GAL URE of 6.9 cm in both correction streams. While the values reported here for some of the individual GAL components are higher than those reported in Naciri et al., 2023, the URE is nevertheless slightly better than the SISRE values for Galileo HAS, which were reported to be 10.8 cm. (Note that SISRE and URE are equivalent metrics used to quantify product quality).

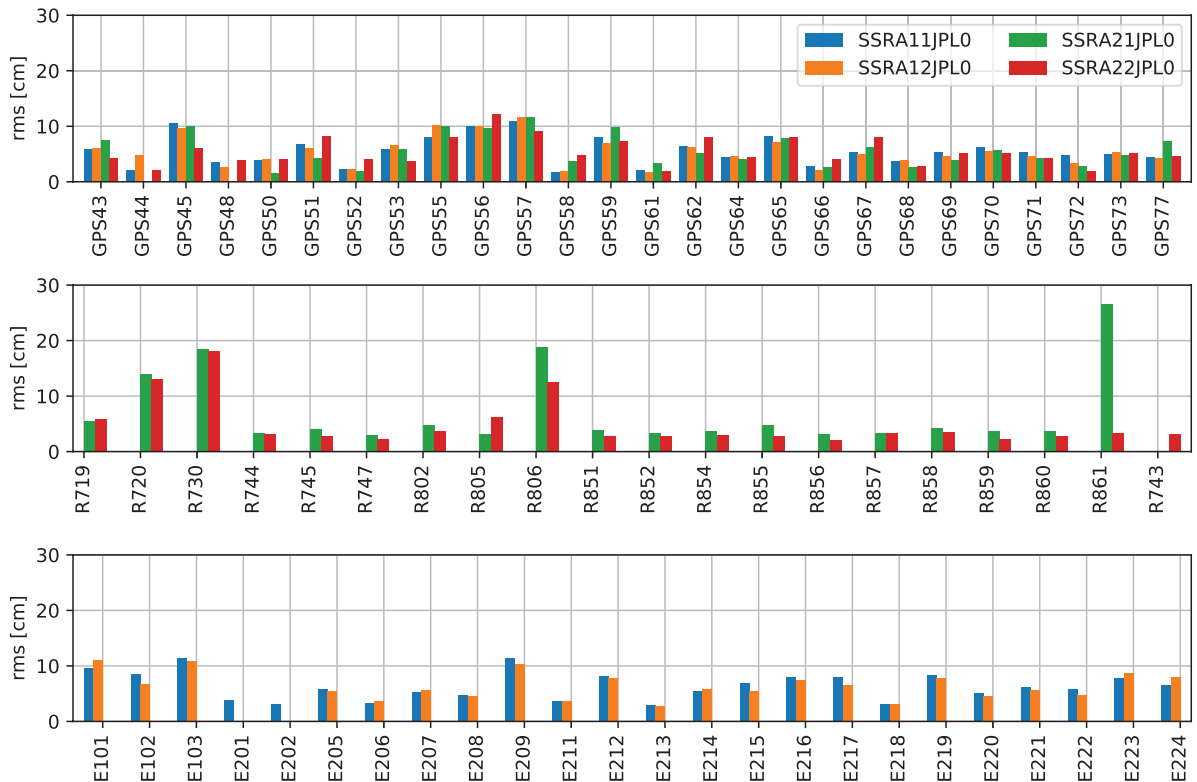


FIGURE 2 URE rms of the GDGPS HAS products compared against final CODE products for a seven-day period, shown separately for each satellite.

The GLONASS corrections are more difficult to compare between different correction streams due to the presence of inter-frequency biases caused by the FDMA structure used by the constellation. These biases often appear as satellite-specific biases in the satellite clocks, which would affect comparisons of GLONASS clocks between two different correction streams. To mitigate this effect, a mean GLONASS clock per satellite was removed per day, based on the assumption that inter-frequency biases vary slowly over the course of a day. However, one consequence of this removal is that the clock differences essentially become standard deviations and only contain the variability between correction streams. This undesired but necessary consequence explains the lower GLONASS clock differences and UREs compared to GPS and Galileo in Table 1. Nonetheless, the two GLONASS streams performed similarly after the outlier satellites were removed, with an rms of approximately 4.8 cm.

These product quality analyses show that all four streams are equivalent after outlier removal and that the GPS and Galileo corrections are comparable to, or even better than, corrections from BeiDou PPP-B2b and Galileo HAS. However, the results in Table 1 are consolidated across all satellites. To understand the performance of each satellite and identify outliers, Figure 2 shows the rms of each satellite's URE over the same seven-day period in autumn 2024 for each correction stream.

Figure 2 complements the results in Table 1, as it shows consistent performance not only across the different correction streams but also across satellites. In the case of GPS, which is the only common constellation among all four streams, each satellite performs similarly across all four streams. GPS also exhibits similar performance among satellites, showcasing the high quality of GPS corrections. In the case of GLONASS, UREs are also low and consistent across satellites and correction streams, as the satellite-dependent biases were removed from each satellite's clock. However, three exceptions can be seen: both GLONASS streams have a higher URE for R730, and the SSRA21JPL0 stream has higher UREs for R806 and R861. The higher R730 UREs arose due to a mismatch in the satellite antenna calibration with CODE and will be fixed in future iterations of the streams. The higher UREs for SSRA21JPL0 for R806 and R861 are well understood and will also be fixed in future iterations of the streams. Finally, the performance of Galileo mirrors that of GPS: for each satellite, both streams perform similarly, and for each stream, UREs are consistent across different satellites. Overall, this comparison of GDGPS HAS to CODE shows that the GDGPS HAS streams exhibit good, consistent performance across streams and satellites, even when compared to similar services such as BeiDou PPP-B2b and Galileo HAS.

3.2 | Long-term analysis of URE

The products analysis in the previous section focused on data collected over a one-week period spanning late September and early October 2024, but long-term performance is also important for understanding the quality of the GDGPS HAS products. Comparisons between URE values and high-precision GipsyX rapid products have been routinely generated and saved over months and can therefore provide a long-term analysis of product quality. In general, CODE orbits and clocks and the GipsyX rapid orbits and clocks are expected to yield similar URE values for real-time correction streams. The box-and-whisker plot in Figure 3 summarizes the long-term behavior of UREs for GPS, as data for other constellations has not been saved. The figure is based on eight months of data, ranging from January 1st, 2024 to September 1st, 2024. Each color represents a different correction stream, as

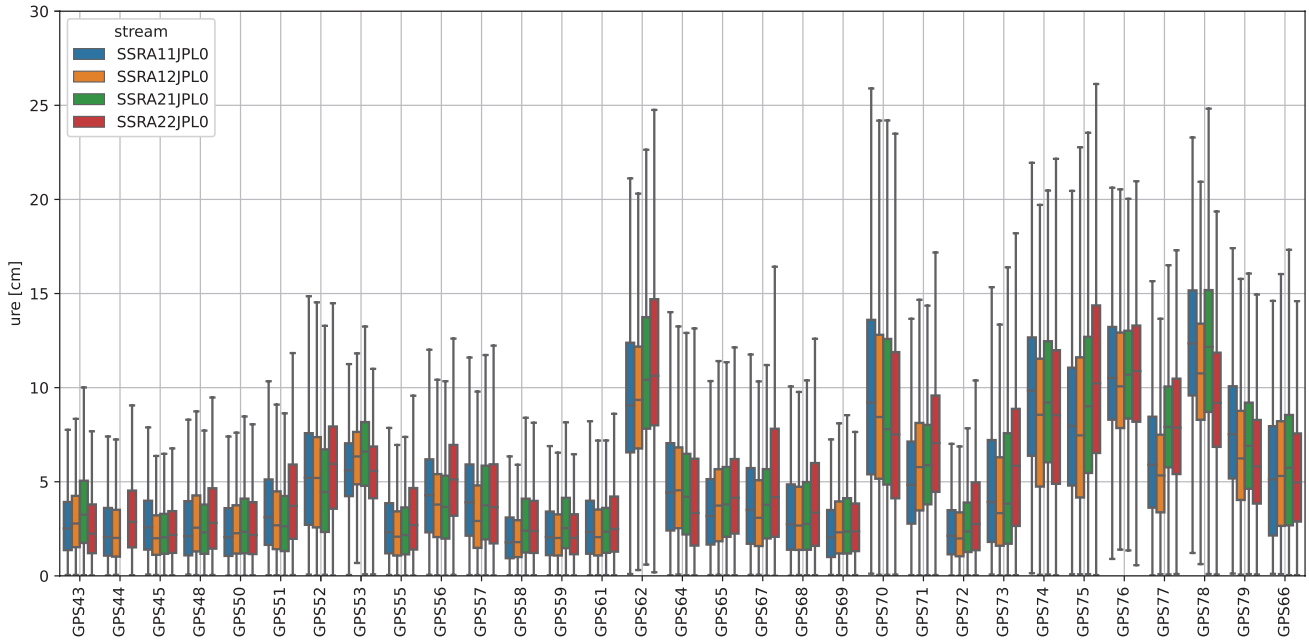


FIGURE 3 Box-and-whisker plot showing the URE for GPS satellites from all four streams. The figure is based on eight months of data between January 1st, 2024 and September 1st, 2024. The UREs are computed at 5-minute intervals relative to GipsyX rapid GPS products.

in Figure 2. For each satellite and stream, the URE distribution is represented by: 1) a minimum URE: the bottom whisker, 2) a maximum URE: the top whisker, 3) a median: the horizontal line inside the box, 4) the first quantile, or 25th percentile: the box's bottom boundary, and 5) the third quantile, or 75th percentile: the box's top boundary.

Overall, Figure 3 shows that URE distributions are comparable between all filters and satellites. With the exception of a select few satellites with higher medians and maximums, the satellites are generally well-behaved, as the median and most third quartile UREs are below 10 cm. These distributions attest to the stability and high quality of GPS products in all four correction streams, agreeing with the earlier comparison against final CODE products. The high quality of the GPS products, along with the high quality of the Galileo and GLONASS products as shown in section 3.1, should directly translate to high-quality user PPP performance.

3.3 | Latency analysis

The correction streams described in this research are all intended for real-time processing rather than file-based processing. As such, the latency of the corrections becomes important, as large delays in the generation and reception of the corrections would lead to higher positioning errors for users (Martin et al., 2015). Quick generation and dissemination of the products is therefore of the utmost importance, with latencies below ten seconds considered optimal for precise positioning (Hadas & Bosy, 2014). Figure 4 shows the latency distribution for each of the correction streams, with the different streams colored as before. In the top panel, POD latency is the time between the nominal observation time and the time at which the precise products are generated by the POD filter, while in the bottom panel, total latency is the time between the nominal observation time and the time at which the precise products are received by the user as broadcast through the IGS.

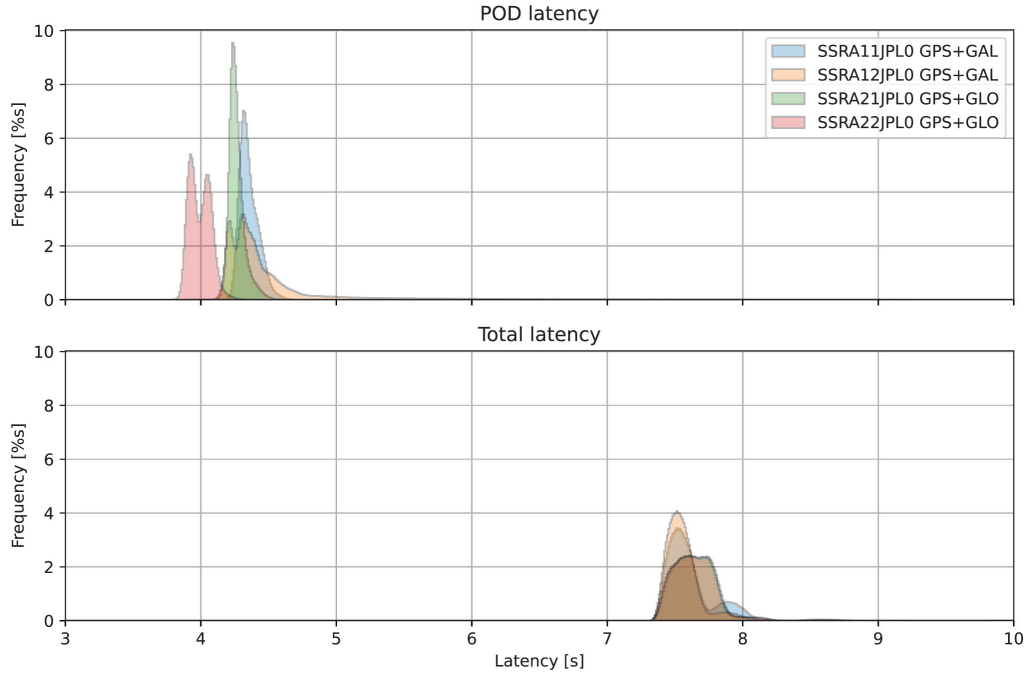


FIGURE 4 Histograms showing the latency from correction generation (top) and the total latency at the user side (bottom) for each individual stream between September 27th, 2024 and October 10th, 2024.

Overall, Figure 4 shows that the GDGPS HAS corrections have a desirably low latency. With the exception of some outliers for the SSRA12JPL0 stream, the latency for correction generation is largely below five seconds. For three of the four streams, the bulk of each latency distribution is slightly over four seconds, and for SSRA22JPL0, most latencies are below four seconds. Moreover, the total latencies from all four streams are between 7 and 8 seconds, which is very reasonable for real-time processing. These distributions demonstrate the low correction latency even at the user level, which is well below the ten-second threshold mentioned above. Assuming any reasonable transfer over the internet or other media, these latencies are sufficiently low to enable precise real-time user positioning.

4 | USER PROCESSING VIA INDEPENDENT SOFTWARE

To assess user performance with the GDGPS HAS correction streams described above, this paper uses the York-PPP engine to process a large number of observation data through each correction stream and then analyzes the PPP results. The following sections describe the York-PPP engine, the PPP model used for analysis, and the data used for user processing.

4.1 | User engine and model

The York-PPP engine is a user positioning engine developed at the GNSS Laboratory in York University, Toronto, Canada. The engine is capable of multi-constellation, multi-frequency processing of GNSS data with the possibility of real-time positioning (Aggrey, 2015; Naciri, 2023; Seepersad, 2018). The engine also has additional processing capabilities, such as an inertial measurement unit and odometer integration or smartphone processing, that are beyond the scope

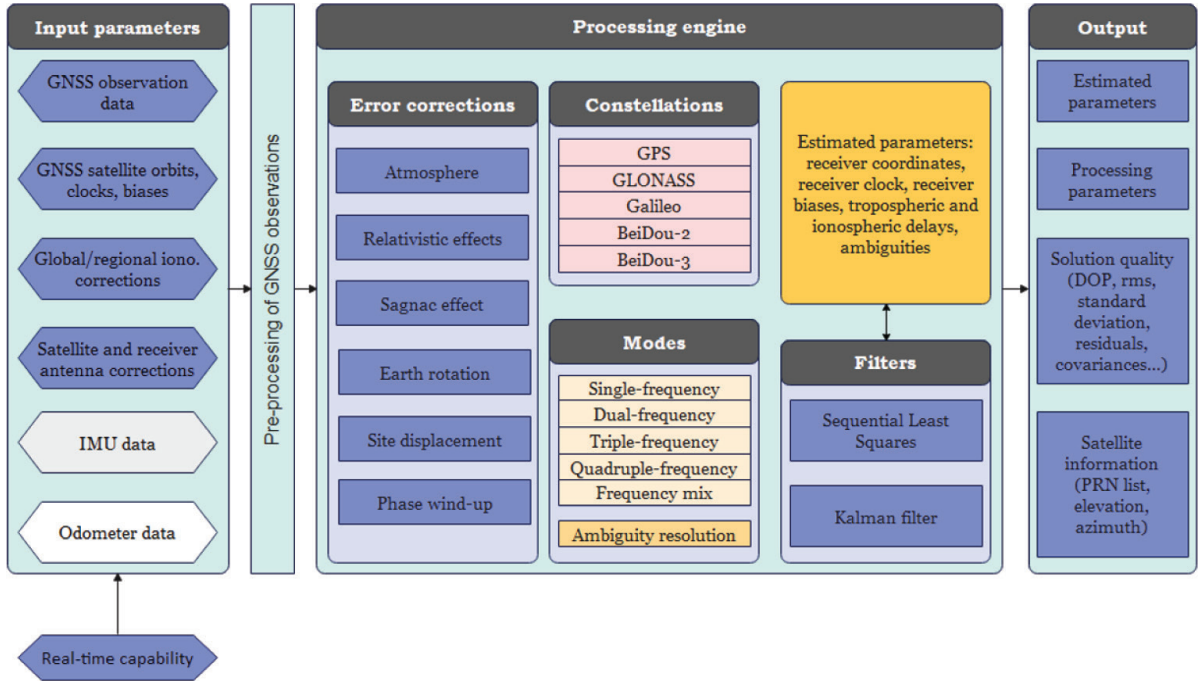


FIGURE 5 High-level diagram of the capabilities of the York-PPP engine used for user processing.

of the current study. The engine supports real-time, simulated real-time, and post-processed data processing using a variety of measurement correction formats. Figure 5 shows a high-level description of the software.

For this research, the York-PPP engine is used for simulated real-time processing of geodetic data with GDGPS HAS correction data, in addition to real-time correction data from CNES and Galileo HAS. The processing is performed on dual-frequency observation data for GPS, Galileo, and GLONASS and is limited to float positioning using only orbits and clocks. To ensure that processing can be replayed and that the corrections streams are archived, the real-time data is streamed and logged using the Federal Agency for Cartography and Geodesy (BKG) NTRIP Client (BNC) software (Stürze et al., 2016). SSR and ephemeris data are logged in ASCII files, which are read by the York-PPP engine and processed in simulated real-time. In other words, files are processed in forward mode using only data that would be available to the user at each epoch in a real-time scenario. As is the case for real-time processing, any latency is embedded in the corrections, but the low latencies shown in Figure 4 have limited effect on user solutions.

Although the York-PPP engine is capable of processing with different PPP models, such as the Decoupled Clock Model (Collins et al., 2010; Naciri & Bisnath, 2021) for PPP-AR, this research uses a simple float model. The float model is based on uncombined processing, using only raw measurements on individual frequencies without forming ionosphere-free combinations. The equation models are shown in Equation (3):

$$\begin{cases} P_1^s = \rho_r^s + c(dt_r - dt^s) + \gamma_1 I_1^s + M_r^s \cdot T_r & + \epsilon_{P_1} \\ P_2^s = \rho_r^s + c(dt_r - dt^s) + \gamma_2 I_1^s + M_r^s \cdot T_r & + \epsilon_{P_2} \\ \Phi_1^s = \rho_r^s + c(dt_r - dt^s) - \gamma_1 I_1^s + M_r^s \cdot T_r + \lambda_1 N_1^s & + \epsilon_{\Phi_1} \\ \Phi_2^s = \rho_r^s + c(dt_r - dt^s) - \gamma_2 I_1^s + M_r^s \cdot T_r + \lambda_2 N_2^s & + \epsilon_{\Phi_2} \end{cases} \quad (3)$$

In Equation (3), for a receiver r and a satellite s , P_i^s and Φ_i^s are the pseudo-range and carrier-phase measurements on frequency $f_i, i \in \{1, 2\}$, and ρ_r^s is the geometric range between the receiver and the satellite. c is the speed of light in a vacuum, and dt_r and dt^s are the receiver and satellite clock offsets, respectively. $\gamma_i = \frac{f_i^2}{f_1^2}$ is the coefficient that maps the L1/E1/G1 ionospheric delay I_1^s to each frequency f_i . M_r^s is the mapping function applied to the zenith wet tropospheric delay T_r . In the latter two equations, λ_i is the wavelength of the signal on frequency f_i , and N_i^s is the corresponding carrier-phase ambiguity. Note that carrier-phase ambiguities contain various receiver- and satellite-dependent biases, as is the nature of float models. For instance, the carrier-phase ambiguities contain the satellite phase biases, which are not corrected for in this research. Finally, ϵ_{p_i} and ϵ_{ϕ_i} are the pseudorange and carrier-phase residuals on frequency f_i , respectively.

4.2 | Test data description

The model described above is used to process observation data collected from a global set of 40 stations that each support L1/L2 for GPS, E1/E5b for Galileo, and G1/G2 for GLONASS. The stations are part of the IGS network and are distributed across all continents, as shown by the black dots labeled *PPP* in Figure 6. In addition to the user PPP stations, Figure 6 also shows stations labeled *POD*, which are used in the network processing to generate the GDGPS HAS SSR corrections. These POD stations are shown to demonstrate the global coverage of the service as well as its high redundancy. Although some PPP stations overlap with the POD stations, most do not. Data from the stations were downloaded from CDDIS in Receiver Independent Exchange (RINEX) format and processed in simulated real-time. The data were collected over the same seven-day period as in the products analysis between late September and early October 2024, and have a 30-second update interval. Each station's data were split into three-hour long data sets, amounting to a total of over 2,000 datasets that are independent in time. RINEX data were used, rather than real-time observation data, to ensure ease of re-processing and avoid any issues related to observation data transmission affecting the PPP results.

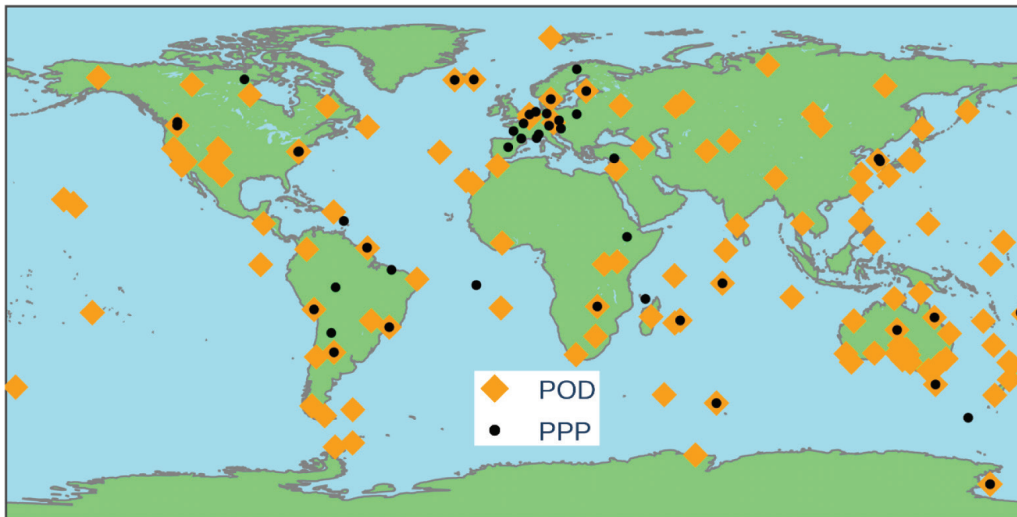


FIGURE 6 Locations of the stations used for precise orbit determination (POD) of the GDGPS HAS corrections and for PPP user processing.

4.3 | Processing strategies

The observation data described above is processed with the York-PPP engine using the different correction streams. The processing strategy was designed to keep the comparisons fair and equitable between all correction streams given the differences in definitions and reference points among the different streams. The full processing strategies are detailed in Table 2. For example, all GDGPS HAS and the Galileo HAS streams have orbits referring to the ionosphere-free antenna phase center of each constellation's primary frequency pair, while orbits for the CNES stream refer to the L1/E1/G1 antenna phase center. Such differences are accounted for when processing user data. Similarly, the primary observables for GDGPS HAS are 1W and 2W for GPS but are 1C and 2W for Galileo HAS. The user engine therefore prioritizes 1W for GDGPS HAS (and CNES) and 1C for Galileo HAS.

Parameter estimation is performed using a sequential least-squares filter, and the stochastic modeling strategy is detailed in Table 2. Despite the stations being static, the receiver positions are estimated with large process noise, which enables an analysis of the kinematic performance without imposing large constraints on user dynamics. In addition, given the existence of inter-constellation biases, one receiver clock is estimated per constellation. Similar measurement weights are used for all constellations except GLONASS, for which the post-fit residual rejection threshold is twice that of other constellations to account for GLONASS's inter-signal biases (Yamada et al., 2010). Other corrections, such as the phase wind-up, relativistic effect, and Earth rotation, are applied following the International Earth Rotation Service (IERS) conventions (Kouba & Mireault, 1998).

TABLE 2
Processing strategy for the estimated parameters

Parameter	Strategy
Observation data	30-second RINEX data from CDDIS
Broadcast ephemeris	Logged from the JPLEPH31 real-time stream
Orbits and clocks	JPL: SSRA11JPL0, SSRA12JPL0, SSRA21JPL0, SSRA22JPL0 CNES: SSRA00CNE0 Galileo HAS: SSRA00EUH0
Receiver coordinates	Estimated with process noise equivalent to 100 km/h
Receiver reference coordinates	IGS SINEX positions
Receiver clock dt_r	Estimated as a white noise process
Tropospheric delay	Dry: global mapping function model and mapping function (Kouba, 2009). Wet: estimated as a random walk process with process noise of $0.05 \text{ mm}/\sqrt{h}$
Ionospheric delays	Estimated as white noise processes
Ambiguities	Estimated as constants on each continuous arc
Elevation angle cut-off	7°
Receiver and satellite antenna corrections	Corrected for using IGS20 ANTEX file
Weighting strategy	Elevation dependent weighting: $\sigma = \frac{\sigma_{90}}{a + b \sin el}$ with σ_{90} equal to 0.1 m and 0.001 m for the pseudorange and carrier-phase measurements, respectively, and el being the elevation angle. a and b are set to 0.15 and 0.85, respectively.

5 | USER PPP RESULTS ANALYSIS

The following section presents the results from an analysis of the global PPP results. The section begins with an analysis of the GDGPS HAS results and then compares the GDGPS HAS performance to that of the CNES and Galileo HAS correction streams.

5.1 | User performance analysis

This section consolidates and summarizes the results from processing the over 2,000 individual three-hour-long datasets for each GDGPS HAS correction stream. User results are analyzed in terms of accuracy and convergence time relative to SINEX reference positions from the IGS. For example, Figure 7 shows the rms time series for each of the GDGPS HAS streams using the same color scheme as before. The figure is generated by computing, on each epoch, the rms of all data sets after removing outliers that have three-dimensional position errors higher than two meters, as these outliers are caused by observation data quality. The removal of such outliers is especially important because no pre-filtering of the observation data was performed prior to PPP processing: in other words, all data from all 40 stations over the seven-day collection window was processed by the PPP engine without prior removal of any problematic observation data. On average, approximately 1% to 2% of the data points were rejected from the rms computation in each epoch. For each stream, Figure 7 compares both a GPS-only solution and a dual-constellation

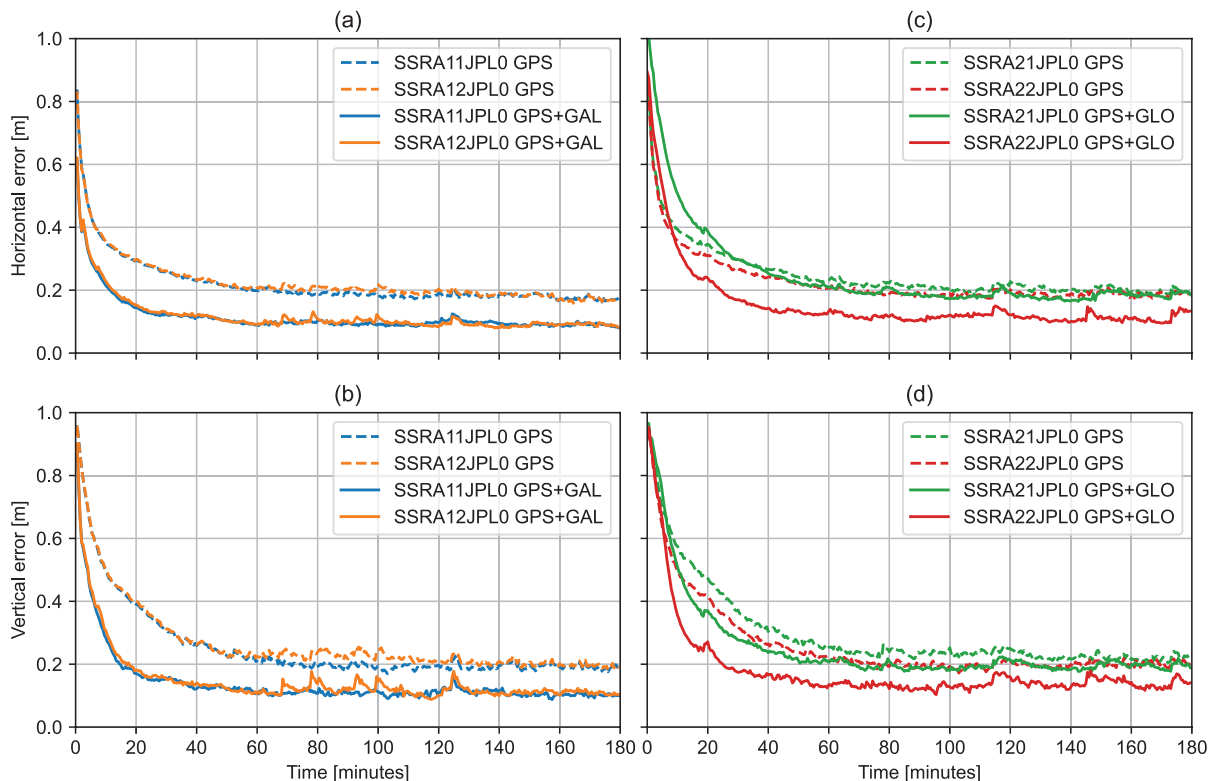


FIGURE 7 rms performance based on all data sets with GDGPS HAS corrections for the GPS+GAL streams (SSRA11JPL0 and SSRA12JPL0) with (a) horizontal and (b) vertical errors, and GPS+GLO streams (SSRA21JPL0 and SSRA22JPL0) with (c) horizontal and (d) vertical errors. For each epoch, each time series is computed as the rms of all horizontal or vertical errors after removal of three-dimensional errors greater than two meters.

solution. Dashed lines represent the single-constellation solutions, while the same-colored solid lines represent their equivalent dual-constellation solutions.

Figure 7 demonstrates how comparable each pair of same-constellation streams is. For example, consider the two GPS+GAL streams (SSRA11JPL0 and SSRA12JPL0, shown in blue and orange). For each pair of single-constellation solutions, the solutions can hardly be distinguished from one another. This overlap between pairs of redundant streams is expected, as URE analysis showed comparable values between SSRA11JPL0 and SSRA12JPL0. However, the two streams exhibit small differences in their dual-constellation solutions. This difference arises due to a discrepancy in the quality of the GLONASS corrections, as illustrated in Figure 3. The difference in GLONASS corrections is well-understood and will be corrected in future versions of the streams. Overall, all four GPS-only solutions produced comparable results, while the GPS+GAL solutions perform better than the GPS+GLO solutions in terms of convergence time and position error. The different performances between the two dual-constellation solutions are likely due to the inter-signal biases from GLONASS. Longer convergence times and higher position errors in a GPS+GLO solution relative to GPS+GAL were similarly observed by (Li & Pan, 2021) using real-time CNES products.

Figure 8 quantifies the horizontal and vertical convergence times and rms for all four dual-constellation solutions shown in Figure 7. The convergence times are defined relative to 20 cm and 40 cm horizontal and vertical error, respectively. These convergence time thresholds are the same as defined for Galileo HAS, as specific thresholds for GDGPS HAS have not yet been defined. The rms are computed between hours one and three of the processing to exclude the convergence period. Consistent with the observations from Figure 7, the two GPS+GAL streams perform similarly, as their respective convergence times and rms overlap: convergence times are 12 minutes and 6.5 minutes horizontally and vertically, respectively, and rms are 13.5 cm and 17.5 cm horizontally and vertically, respectively. In contrast, the SSRA22JPL0 GLONASS stream performs better than SSRA21JPL0: the convergence times for SSRA22JPL0 are 24.5 minutes and 9.0 minutes horizontally and vertically, respectively, whereas the vertical convergence time for SSRA21JPL0 is 15.5 minutes. Moreover, SSRA21JPL0 does not converge below 20 cm horizontally, as the solution settles around that threshold. In terms of rms, SSRA21JPL0 has horizontal and vertical rms of 28.4 cm and 28.6 cm, respectively, as opposed to 19.5 cm

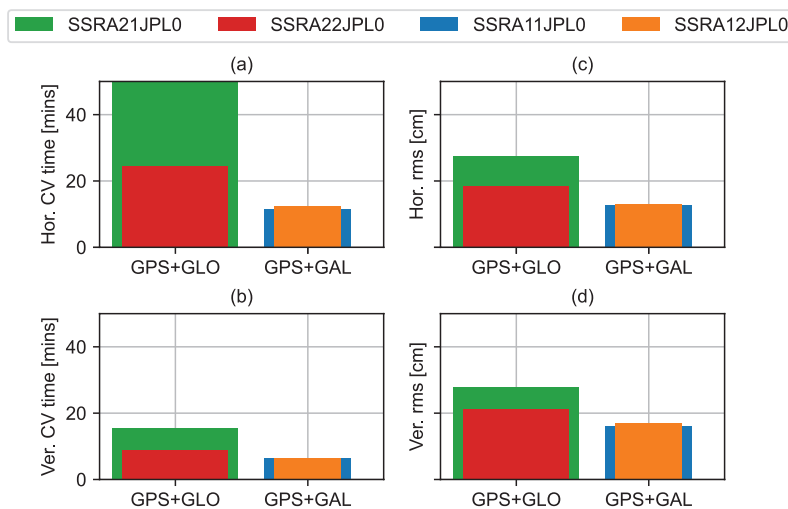


FIGURE 8 Statistics for the multi-GNSS time series shown in Figure 7. Horizontal (a) and vertical (b) convergence times are relative to 20 cm and 40 cm errors, respectively, and horizontal (c) and vertical (d) rms are computed between the first and third hours of processing.

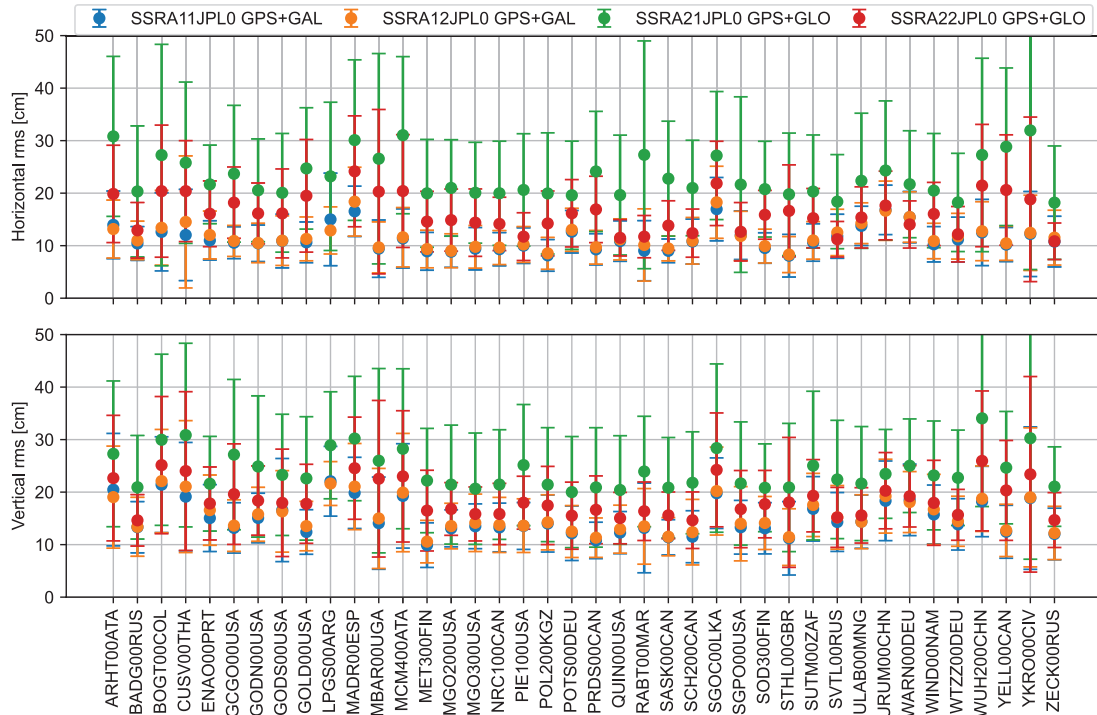


FIGURE 9 Per-station performance of the dual-constellation GDGPS HAS results. Dots represent the mean rms across each station’s 56 data sets, and error bars represent the corresponding standard deviations. Rms are computed over the whole duration of the processing after removal of three-dimensional position errors greater than two meters.

and 22.2 cm for SSRA22JPL0. Overall, considering that these solutions involve two constellations and do not involve any ambiguity resolution, these results show very good performance. The equivalence between both GPS+GAL streams supports the use of parallel GPS+GAL streams, while the differences between the two GPS+GLO streams are well-understood and will be removed in future iterations of the streams.

Figures 7 and 8 show the overall performance based on all data sets, so to better understand the global coverage from the service, Figure 9 shows the performance per station. Figure 9 is generated by (i) computing the total rms of each individual three-hour dataset after removing three-dimensional position errors greater than two meters and then (ii) computing the mean and standard deviation of these rms for each station. Dots represent the mean rms for each station, while error bars represent the standard deviation. Streams are colored as before. As can be seen in the figure, for each stream, performance is consistent across all stations. The GPS+GAL solutions are comparable between the SSRA11JPL0 and SSRA12JPL0 streams and have lower standard deviations compared to the GPS+GLO solutions, showing that, for each station, the GPS+GAL results are consistent over time. The larger standard deviations of the GPS+GLO solutions are likely due to the three GLONASS satellites with high UREs shown in Figure 3.

5.2 | Direct comparison against external correction streams

To put these different GDGPS HAS results in context, this section compares the GDGPS HAS results against solutions generated from other correction streams: CNES and Galileo HAS. The CNES and Galileo HAS streams are logged in

real-time, like GDGPS HAS, and their data are used to process the same observation data as GDGPS HAS. Definition discrepancies such as different reference antenna points, as well as different frequency combinations, are accounted for as discussed in Section 4.3.

5.2.1 | Comparison of GPS+GLO streams against CNES

The two GPS+GLO streams are first analyzed by comparison to the real-time CNES stream. CNES provides multi-GNSS (GPS, GLONASS, Galileo, BeiDou) corrections in their SSR streams, so, to allow for a fair comparison, a dual-constellation solution using only GPS and GLONASS was generated using CNES corrections and then compared to the solutions from the two GPS+GLO GDGPS HAS streams, as shown in Figure 10. The figure displays the cumulative distributions of the rms for individual three-hour datasets, for each of the three solutions. The rms are computed between hours two and three of processing for each data set to eliminate any convergence period, and the two GDGPS HAS streams are colored as before. As expected from the user performance analysis described above, the SSRA22JPL0 stream performed better than SSRA21JPL0: approximately 95% of the datasets have horizontal rms below 20 cm and 84% have horizontal rms below 10 cm for SSRA22JPL0, as opposed to approximately 88% and 70%, respectively, for SSRA21JPL0. In comparison, the CNES solution performs similarly to the poorer-performing SSRA21JPL0, with the former having a slightly better distribution. Indeed, only 86% of CNES solutions have horizontal rms below 20 cm, and 74% are below 10 cm. The figure attests to the quality and performance of the GDGPS HAS GPS+GLO streams relative to other well-established products such as those from CNES.

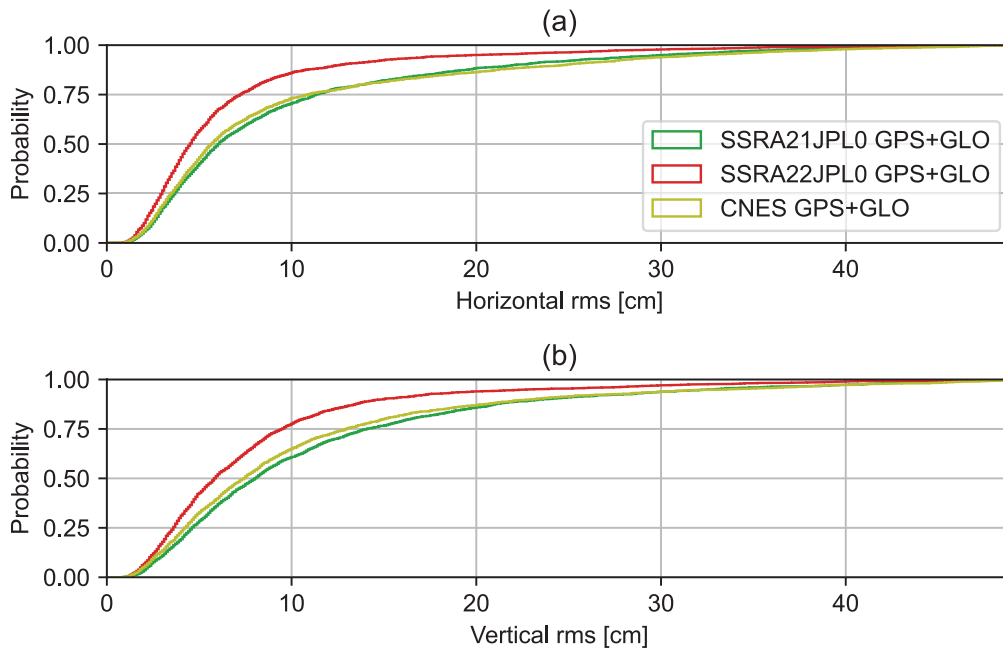


FIGURE 10 Comparison of the horizontal (a) and vertical (b) position cumulative distributions using GPS+GLO GDGPS HAS and CNES correction streams on the data described in section 4.2. The distributions are based on the rms of each three-hour dataset between hours two and three to eliminate any convergence period.

5.2.2 | Comparison of GPS+GAL streams against Galileo HAS and CNES

Here, the rms distribution for the GPS and Galileo streams is compared to external solutions from both CNES and Galileo HAS. All four solutions (two GDGPS HAS, one CNES, and one Galileo HAS) use the same observation data and similar processing strategies based on GPS+GAL processing. The results are summarized in Figure 11, with the GDGPS HAS streams colored as before.

As in the user performance analysis, the two GDGPS HAS streams produced equivalent results with overlapping distributions. Compared to the external solutions, the GDGPS HAS streams were comparable to the CNES solution and better than Galileo HAS. Overall, the results show the high quality of the GPS+GAL solutions, as over 97% and 90% of data sets have a horizontal rms lower than 20 cm and 10 cm, respectively. For the CNES solution, 93% of solutions have a horizontal rms below 20 cm, while 77% have a horizontal rms below 10 cm. In contrast, only 86% of datasets have a horizontal rms below 20 cm horizontally for Galileo HAS, and only 47% are below 10 cm. The considerably better performance of GDGPS HAS and CNES relative to Galileo HAS is attributed to the large number of ground stations used to generate the corrections for GDGPS HAS and CNES. Galileo HAS currently uses only 14 reference stations (Fernandez-Hernandez et al., 2022), though additional Galileo tracking stations will be added in the near future, and some of the user stations in the Pacific region fall outside Galileo HAS's current coverage area. Overall, these comparisons against CNES and Galileo HAS demonstrate that the GDGPS HAS results are of high quality and perform comparably to other high-quality correction streams. Moreover, because these results are based on float dual-frequency dual-constellation solutions, they could be further improved by incorporating additional frequencies or constellations or even through the use

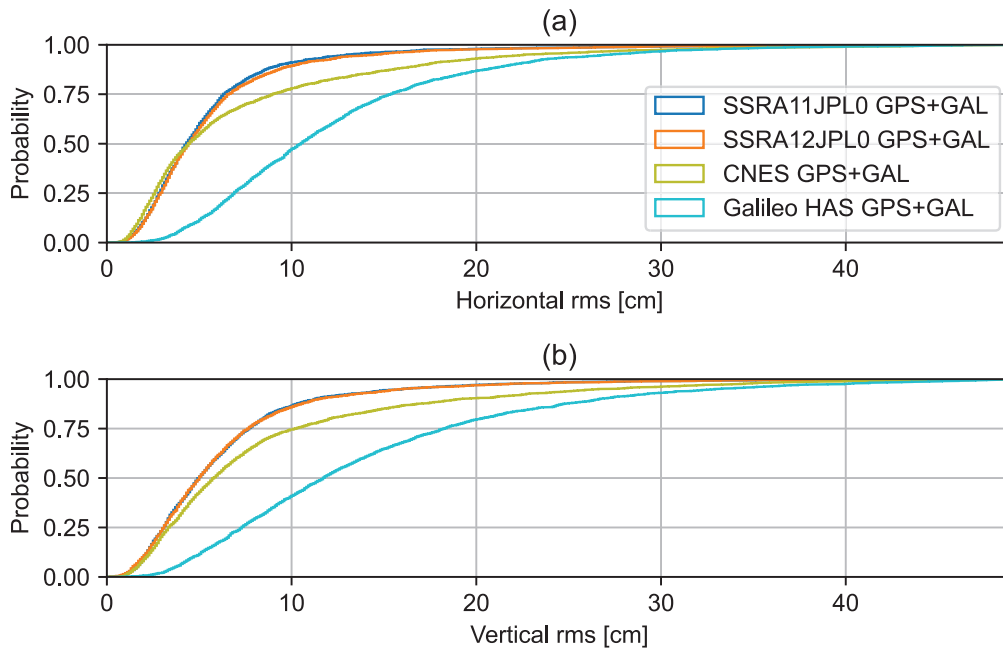


FIGURE 11 Comparison of the horizontal (a) and vertical (b) position cumulative distributions using GPS+GAL GDGPS HAS, CNES, and Galileo HAS correction streams on the data described in section 4.2. The distributions are based on the rms of each three-hour dataset between hours two and three to eliminate any convergence period.

of ambiguity resolution once satellite pseudorange and carrier-phase biases are made available.

5.2.3 | Consolidation of PPP results

To summarize the PPP results shown in this paper and provide a single comparison with external correction streams, Figure 12 shows the average time series for each PPP solution described herein together with their standard deviations. The figure for each solution is generated by computing, at each epoch, the mean and standard deviation of the position errors for all 2,100 datasets after removing three-dimensional position errors greater than two meters. The first column shows the GPS+GAL solutions, while the second column shows the GPS+GLO solutions. The first two rows contain the GDGPS HAS solutions, and the third and fourth contain the CNES and Galileo HAS solutions.

This overall synthesis reaffirms that each pair of GDGPS HAS solutions performs comparably and that the GPS+GLO solutions have larger means and standard deviations than the GPS+GAL solutions. As noted earlier, the lower GPS+GLO performance can be attributed to the presence of unaccounted-for inter-frequency biases in GLONASS, the absence of code biases in the SSR streams, and the well-known higher UREs for three satellites that will be accounted for in future iterations. The GDGPS HAS streams for both the GPS+GLO and GPS+GAL solutions perform comparably to CNES, as both means and scatters in the CNES solutions are similar to GDGPS HAS. Finally, Galileo HAS has a higher mean and standard deviation compared to the other GPS+GAL solutions, likely due to the more limited number of ground stations it used for correction estimation.

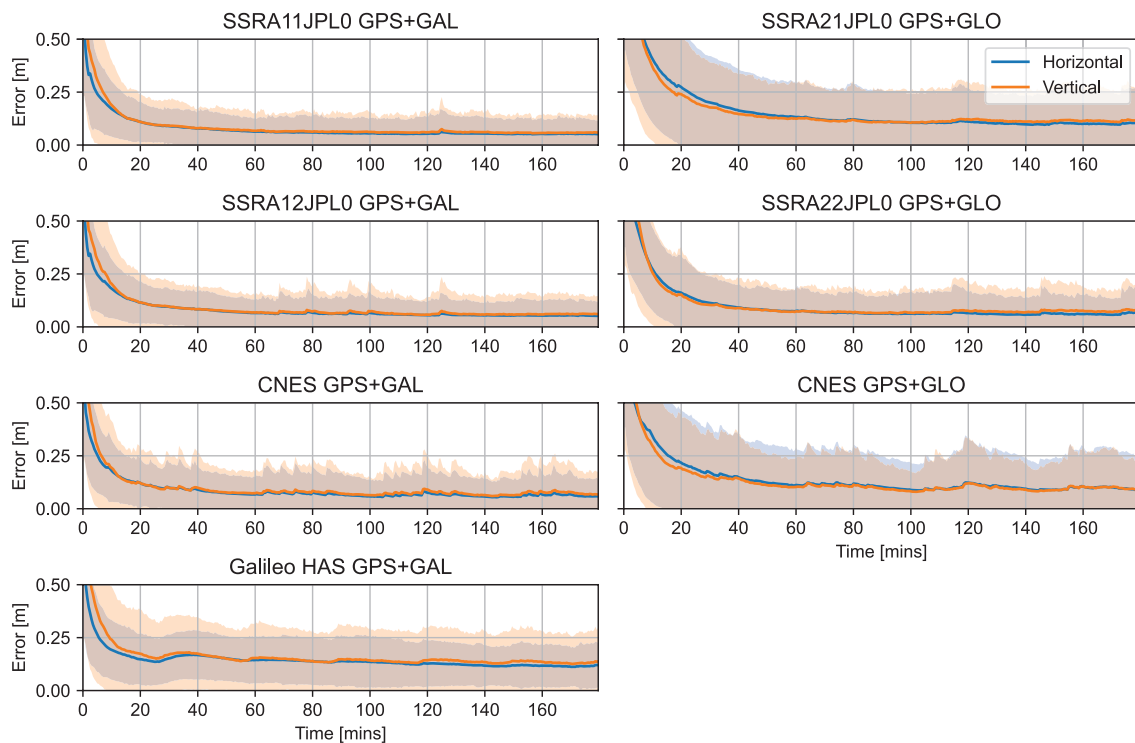


FIGURE 12 Comparison of the epoch-wise position error means and standard deviations based on all datasets using the various GDGPS HAS and external correction streams. Outliers with three-dimensional position errors greater than two meters are removed.

6 | CONCLUSIONS

GPS has long been the pioneer in satellite-based positioning. Its development and large-scale adoption by civilian applications have led to an increased reliance on it, spurring new constellations such as Europe's Galileo and China's BeiDou. However, these new constellations provide services that are not supported by GPS, such as high-accuracy services that enable decimeter- to centimeter-level positioning using only signals broadcast by the GNSS constellations. Although GPS provides no such service directly, an equivalent service could potentially be provided through an internet distribution of the corrections generated by JPL's GDGPS System. This paper considered a GDGPS-based HAS in the form of six different streams: two parallel streams containing broadcast ephemeris for GPS, Galileo, and GLONASS; two parallel streams containing 1 Hz SSR corrections for GPS and Galileo; and two parallel streams containing 1 Hz SSR corrections for GPS and GLONASS. Each flavor of stream is generated by completely independent infrastructure to ensure reliability through redundancy. The results shown herein demonstrate the high quality of the corrections, with UREs of 6 cm to 6.4 cm for GPS on all four streams, 6.9 cm for Galileo for both GPS+GAL streams, and approximately 4.8 cm for GLONASS for both GPS+GLO streams. However, the GLONASS UREs are not representative because a satellite mean was removed during processing to account for the presence of inter-signal biases. These high-quality products performed consistently over a period of eight months and can be promptly delivered to users, with correction generation latencies below 5 seconds and total latencies at the user level below 8 seconds. The high quality of these products translates directly into user positioning results, as evidenced by PPP solutions generated by an independent user engine from York University's GNSS Laboratory. Results show that the GDGPS HAS solutions are comparable to solutions based on CNES real-time products, and that the GPS+GAL streams perform better than the Galileo HAS internet-based streams due to their larger number of network stations. The promising performance from GDGPS HAS may be further enhanced in future iterations that include support for code and phase biases and for additional frequencies, along with potential ionospheric corrections to reduce convergence times.

ACKNOWLEDGMENTS

Work from all GDGPS contributors is acknowledged in developing the technology that enables GDGPS HAS. The research was carried out at the Jet Propulsion Laboratory, California Institute of Technology, under a contract with the National Aeronautics and Space Administration. Funding sources include the NASA Science Mission Directorate's Space Geodesy Program and the Natural Sciences and Engineering Research Council of Canada (NSERC).

CONFLICT OF INTEREST

The authors declare no potential conflict of interests.

REFERENCES

- Aggrey, J. E. (2015). *Multi-GNSS precise point positioning software architecture and analysis of GLONASS pseudorange biases* [Master's Thesis, York University]. YorkSpace. <http://hdl.handle.net/10315/29969>
- Bar-Sever, Y., Komjathy, A., Mannucci, A., & Oria, A. (2022). *The global differential GPS (GDGPS) system: Architecture, capabilities, and operations*. <https://doi.org/10.48577/jpl.PZWW70>
- Bertiger, W. L., Bar-Sever, Y. E., Haines, B. J., Iijima, B. A., Lichten, S. M., Lindqwister, U. J., Mannucci, A. J., Muellerschoen, R. J., Munson, T. N., Moore, A. W., Romans, L. J., Wilson, B. D., Wu, S. C., Yunck, T. P., Piesinger, G., & Whitehead, M. (1997). A real-time wide area differential GPS system. *NAVIGATION*, 44(4), 433–447. <https://doi.org/10.1002/j.2161-4296.1997.tb02359.x>

- Bertiger, W., Bar-Sever, Y., Dorsey, A., Haines, B., Harvey, N., Hemberger, D., Heflin, M., Lu, W., Miller, M., Moore, A. W., Murphy, D., Ries, P., Romans, L., Sibois, A., Sibthorpe, A., Szilagyi, B., Vallisneri, M., & Willis, P. (2020). GipsyX/RTGx, a new tool set for space geodetic operations and research. *Advances in Space Research*, 66(3), 469–489. <https://doi.org/10.1016/j.asr.2020.04.015>
- Chen, Y. K., Chien, J.-S., Ghassemi, K., Simundich, T., Taylor, J., & Nyema, N. (2002). User range error evolution and projected performance. *Proc. of the 15th International Technical Meeting of the Satellite Division of the Institute of Navigation (ION GPS 2002)*, Portland, OR, 1575–1584. <https://www.ion.org/publications/abstract.cfm?articleID=2169>
- Collins, P., Bisnath, S., Lahaye, F., & Héroux, P. (2010). Undifferenced GPS ambiguity resolution using the decoupled clock model and ambiguity datum fixing. *NAVIGATION*, 57(2), 123–135. <https://doi.org/10.1002/j.2161-4296.2010.tb01772.x>
- Dach, R., Schaer, S., Arnold, D., Kalarus, M. S., Prange, L., Stebler, P., Jäggi, A., & Villiger, A. (2020). CODE final product series for the IGS. University of Bern. <https://doi.org/10.7892/boris.75876.4>
- EUSPA. (2023). Galileo high accuracy service goes live! <https://www.euspa.europa.eu/newsroom-events/news/galileo-high-accuracy-service-goes-live>
- Falcone, M., Hahn, J., & Burger, T. (2017). Galileo. In P. J. G. Teunissen & O. Montenbruck (Eds.), *Springer handbook of global navigation satellite systems*, 247–272. Springer, Cham. https://doi.org/10.1007/978-3-319-42928-1_9
- Fernandez-Hernandez, I., Chamorro-Moreno, A., Cancela-Diaz, S., Calle-Calle, J. D., Zoccarato, P., Blonski, D., Senni, T., de Blas, F. J., Hernández, C., Simón, J., & Mozo, A. (2022). Galileo high accuracy service: Initial definition and performance. *GPS Solutions*, 26(3), 65. <https://doi.org/10.1007/s10291-022-01247-x>
- GDGPS. (2020). *The global differential GPS system*. Jet Propulsion Laboratory. <https://www.gdgps.net/>
- GLONASS IAC. (n.d.). About GLONASS. GLONASS IAC. https://glonass-iac.ru/en/about_glonass/
- GPS.gov. (2021). *Selective availability*. U.S. Department of Transportation. <https://www.gps.gov/systems/gps/modernization/sa/>
- Hadas, T., & Bosy, J. (2014). IGS RTS precise orbits and clocks verification and quality degradation over time. *GPS Solutions*, 19, 1–13. <https://doi.org/10.1007/s10291-014-0369-5>
- Håkansson, M., Jensen, A. B., Horemuz, M., & Hedling, G. (2017). Review of code and phase biases in multi-GNSS positioning. *GPS Solutions*, 21(3), 849–860. <https://doi.org/10.1007/s10291-016-0572-7>
- IGS. (2023). *Real-time service (RTS)*. <https://igs.org/rts/>
- Kawate, K., Igarashi, Y., Yamada, H., Akiyama, K., Okeya, M., Takiguchi, H., Murata, M., Sasaki, T., Matsushita, S., Miyoshi, S., Miyoshi, M., & Kogure, S. (2023). MADOCA: Japanese precise orbit and clock determination tool for GNSS. *Advances in Space Research*, 71(10), 3927–3950. <https://doi.org/10.1016/j.asr.2023.01.060>
- Kouba, J. (2009). Testing of global pressure/temperature (GPT) model and global mapping function (GMF) in GPS analyses. *Journal of Geodesy*, 83(3-4), 199–208. <https://doi.org/10.1007/s00190-008-0229-6>
- Kouba, J., & Mireault, Y. (1998). *[IGSMail-1943] New IGS ERP format (version 2)*. <https://lists.igs.org/pipermail/igsmail/1998/003315.html>
- Li, X., & Pan, L. (2021). Precise point positioning with almost fully deployed BDS-3, BDS-2, GPS, GLONASS, Galileo and QZSS using precise products from different analysis centers. *Remote Sensing*, 13(19). <https://doi.org/10.3390/rs13193905>
- Liu, C., Gao, W., Liu, T., Wang, D., Yao, Z., Gao, Y., Nie, X., Wang, W., Li, D., Zhang, W., Wang, D., & Rao, Y. (2020). Design and implementation of a BDS precise point positioning service. *NAVIGATION*, 67(4), 875–891. <https://doi.org/10.1002/navi.392>
- Lundberg, O. (1995). Civil GNSS: The Inmarsat vision for the 21st century. *The Journal of Navigation*, 48(2), 166–174. <https://doi.org/10.1017/S0373463300012625>
- Martin, A., Hadas, T., Dimas, A., Anquela, A., & Berne, J. (2015). Influence of real-time products latency on kinematic PPP results. *Proc. of the ESA 5th International Colloquium on Scientific and Fundamental Aspects of the Galileo Program*, Braunschweig, Germany, 27–29. https://www.researchgate.net/publication/311495241_Influence_of_Real-time_Products_Latency_on_Kinematic_PPP_Results
- Miya, M., Fujita, S., Sato, Y., Ota, K., Hirokawa, R., & Takiguchi, J. (2016). Centimeter level augmentation service (CLAS) in Japanese quasi-zenith satellite system, its user interface, detailed design, and plan. *Proc. of the 29th International Technical Meeting of the Satellite Division of the Institute of Navigation (ION GNSS+)*, Portland, OR, 2864–2869. <https://doi.org/10.33012/2016.14644>
- Naciri, N. (2023). *Global, instantaneous, centimetre, satellite-based positioning with precise point positioning* [Doctoral dissertation, York University]. YorkSpace. <https://hdl.handle.net/10315/41327>

- Naciri, N., & Bisnath, S. (2021). An uncombined triple-frequency user implementation of the decoupled clock model for PPP-AR. *Journal of Geodesy*, 95(5), 60. <https://doi.org/10.1007/s00190-021-01510-y>
- Naciri, N., Yi, D., Bisnath, S., de Blas, F. J., & Capua, R. (2023). Assessment of Galileo high accuracy service (HAS) test signals and preliminary positioning performance. *GPS Solutions*, 27(2), 73. <https://doi.org/10.1007/s10291-023-01410-y>
- NASA. (2023). *GPS - NASA [Section: Space Communications & Navigation Program]*. NASA. <https://www.nasa.gov/directorates/somd/space-communications-navigation-program/gps/>
- Seepersad, G. G. (2018). *Improving reliability and assessing performance of global navigation satellite system precise point positioning ambiguity resolution* [Doctoral dissertation, York University]. YorkSpace. <https://yorkspace.library.yorku.ca/xmlui/handle/10315/35570>
- Stürze, A., Mervart, L., Weber, G., Rülke, A., Wiesensarter, E., & Neumaier, P. (2016). The new version 2.12 of BKG Ntrip Client (BNC). *Proc. of the European Geosciences Union General Assembly 2016*, Vienna, Austria. <https://ui.adsabs.harvard.edu/abs/2016EGUGA..1812012S/abstract>
- Swift Navigation. (2020). Swift Navigation, Deutsche Telekom, Ericsson and Quectel announce new vision for supporting 3GPP SSR standard. <https://www.globenewswire.com/news-release/2020/06/30/2055685/0/en/Swift-Navigation-Deutsche-Telekom-Ericsson-and-Quectel-Announce-New-Vision-for-Supporting-3GPP-SSRStandard.html>
- Tang, C., Hu, X., Chen, J., Liu, L., Zhou, S., Guo, R., Li, X., He, F., Liu, J., & Yang, J. (2022). Orbit determination, clock estimation and performance evaluation of BDS-3 PPP-B2b service. *Journal of Geodesy*, 96(9), 60. <https://doi.org/10.1007/s00190-022-01642-9>
- Villiger, A. (2022). [IGSMail-8238] Upcoming switch to IGS20/igs20.atx and repro3 standards. <https://lists.igs.org/pipermail/igsmail/2022/008234.html>
- Wang, N., Yuan, Y., Li, Z., Montenbruck, O., & Tan, B. (2016). Determination of differential code biases with multi-GNSS observations. *Journal of Geodesy*, 90(3), 209–228. <https://doi.org/10.1007/s00190-015-0867-4>
- Whitehead, M. L., Penno, G., Feller, W. J., Messinger, I. C., Bertiger, W. I., Muellerschoen, R. J., Iljima, B. A., & Piesinger, G. (1998). A close look at Satloc's real-time WADGPS system. *GPS Solutions*, 2(2), 46–63. <https://doi.org/10.1007/PL00000036>
- Yamada, H., Takasu, T., Kubo, N., & Yasuda, A. (2010). Evaluation and calibration of receiver inter-channel biases for RTKGPS/GLONASS. *Proc. of the 23rd International Technical Meeting of the Satellite Division of the Institute of Navigation (ION GNSS 2010)*, Portland, OR, 1580–1587. <https://www.ion.org/publications/abstract.cfm?articleID=9276>
- Yang, Y., Gao, W., Guo, S., Mao, Y., & Yang, Y. (2019). Introduction to BeiDou-3 navigation satellite system. *NAVIGATION*, 66(1), 7–18. <https://doi.org/10.1002/navi.291>

How to cite this article: Naciri, N., Bar-Sever, Y., Bertiger, W., Bisnath, S., Komjathy, A., Miller, M., Romans, L., Szilagyi, B., & Vallisneri, M. (2025). Analysis of a high accuracy service based on JPL's global differential GPS. *NAVIGATION*, 72(1). <https://doi.org/10.33012/navi.686>